Supplement of Atmos. Chem. Phys., 23, 417–430, 2023
https://doi.org/10.5194/acp-23-417-2023-supplement

Atmospheric Chemistry and Physics
Open Access

Supplement of

SO_2 enhances aerosol formation from anthropogenic volatile organic compound ozonolysis by producing sulfur-containing compounds

Zhaomin Yang et al.

Correspondence to: Lin Du (lindu@sdu.edu.cn)

S1. Estimation of wall losses of organic vapors

(a) Gas-wall equilibrium. The wall-loss process of gas-phase products is generally taken into account to be first-order and the first-order wall-loss coefficient of gas-phase products, k_w (s^{-1}), can be calculated as

$$k_w = \frac{A}{V} \times \frac{0.25\alpha_w\bar{c}}{1.0 + \frac{\pi}{2} \times \frac{\alpha_w\bar{c}}{4(k_e D_{gas})^{0.5}}} \quad \text{(S1)}$$

where A/V (5.55 m^{-1}) is the surface to volume ratio of Teflon reactor; α_w is the mass accommodation coefficient of gas-phase products onto the inner wall and an α_w value of 10^{-5} was employed (Matsunaga and Ziemann, 2010; Zhang et al., 2014); $\bar{c}$ (m s^{-1}) is the molecules' mean thermal speed; k_e (s^{-1}) and D_{gas} (m^2 s^{-1}) are the eddy diffusion coefficient and the molecular diffusivity, respectively. A k_e value of 0.02 s^{-1} was adopted (Mcmurry and Grosjean, 1985). D_{gas} was estimated to be 6×10^{-6} m^2 s^{-1} (Krechmer et al., 2017; Tang et al., 2015). MW (g mol^{-1}) is molecular weight of the given gas-phase product. An average molecular weight of 200 g mol^{-1} for gas-phase products was used to estimate the influence of vapor wall loss (Sarrafzadeh et al., 2016).

The mean thermal speed could be determined according to the following equation:

$$\bar{c} = \sqrt{\frac{8RT}{\pi MW}} \quad \text{(S2)}$$

where R (8.314 J mol^{-1} K^{-1}) and T (K) are the ideal gas constant and experimental temperature, respectively.

The time required to approach gas-wall equilibrium ($\tau_{g\text{-}w}$, s) can be calculated as:

$$\tau_{g\text{-}w} = \frac{1}{k_w} \quad \text{(S3)}$$

(b) Gas-particle equilibrium. The time associated with approaching gas-particle equilibrium ($\tau_{g\text{-}p}$, s) can be determined using the following equation:

$$\tau_{g\text{-}p} = \frac{1}{2\pi N_p \overline{D_p}\, D_{gas} \overline{F_{FS}}} \quad \text{(S4)}$$

where N_p (# m^{-3}) and $\overline{D_p}$ (m) are the number concentration and mean diameter of aerosol particles, respectively; D_{gas} (m^2 s^{-1}) is the molecular diffusivity. $\overline{F_{FS}}$ is the Fuchs-Sutugin correction and it is equal to:

$$\overline{F_{FS}} = \frac{0.75\alpha_p(1+k_n)}{k_n^2 + k_n + 0.283k_n\alpha_p + 0.75\alpha_p} \quad \text{(S5)}$$

where α_p is the mass accommodation coefficient of gas-phase products onto aerosol particles. An α_p value of 0.7 was adopted (Krechmer et al., 2017). K_n is the Knudsen number, which can be calculated as:

$$k_n = \frac{2\lambda}{D_p} \quad \text{(S6)}$$

The gas mean free path (λ, nm) of gas-phase product is defined as:

$$\lambda = \frac{3D_{gas}}{\bar{c}} \quad \text{(S7)}$$

The value of $\tau_{g\text{-}w}$ was determined to be around 20.4 ± 0.01 min. The estimated $\tau_{g\text{-}p}$ value decreased from 0.13 ± 0.01 to 0.07 ± 0.01 min when SO_2 concentrations increased from 0 to 192 ppb. Gas-particle partitioning could dominate the wall deposition of gas-phase products for particle number concentrations in our chamber experiments.

Table S1. IR absorption of functional groups.

Assignment	Wavenumber (cm^{-1})	References
H-bonding of OH in alcohol	3600–3200	(Hung et al., 2013)
H-bonding of carboxylic acid	3200–2400	(Sax et al., 2005)
aliphatic CH	3000–2800	(Sax et al., 2005)
C=O in carboxylic acid/ketone/aldehyde/ester	1750–1685	(Hung et al., 2013)
OH of alcohol in-plane deformation vibration	1440–1260	
C-O stretching in primary alcohol	1090–1000	
C-O stretching in secondary alcohol	1150–1075	
C-O stretching in tertiary alcohol	1210–1100	
C-O stretching in carboxylic acid	1320–1210	
C-O stretching in peroxide	1150–1030	
asymmetric SO_2 stretching	1415–1370	(Tammer, 2004)
C-O-C stretching	1050–1010	(Liu et al., 2015)
C-O-C stretching in acetal	1085	(Lal et al., 2012)
symmetric SO_2 stretching	1064	(Lal et al., 2012)
C-O vibration of C-O-S	1050–1030	(Hung et al., 2013)
asymmetric SO stretching	1020–850	(Hung et al., 2013)
C-O-C stretching in ether	950	(Lin et al., 2014)
O-O stretching in peroxide	900–800	(Hung et al., 2013)
asymmetric C-O-S stretching	875	(Tammer, 2004)
symmetric C-O-S stretching	750	

Table S2. Measured organosulfur species in cyclooctene SOA using UHPLC/ESI-Orbitrap HRMS.

[M-H]$^-$	**Retention time**	**Error**	**DBE**	**Suggested formula**
m / z	**min**	**ppm**		
226.98682	4.01	0.46389	2	$C_5H_7O_8S^-$
209.01248	6.35	-0.24056	2	$C_6H_9O_6S^-$
225.00740	5.33, 5.63, 6.35, 6.84	-0.20469	2	$C_6H_9O_7S^-$
241.00240	5.52, 5.65	0.14299	2	$C_6H_9O_8S^-$
179.03860	17.27	1.40699	1	$C_6H_{11}O_4S^-$
211.02786	10.29	-1.51393	1	$C_6H_{11}O_6S^-$
227.02313	5.12	0.15723	1	$C_6H_{11}O_7S^-$
197.04898	10.66	0.32085	0	$C_6H_{13}O_5S^-$
213.04335	12.62	-2.26184	0	$C_6H_{13}O_6S^-$
253.00226	5.67, 6.71, 7.34	-0.40659	3	$C_7H_9O_8S^-$
223.02812	8.49, 15.45	0.14111	2	$C_7H_{11}O_6S^-$
239.02309	7.61, 7.87, 9.75	-0.04218	2	$C_7H_{11}O_7S^-$
255.07182	7.57, 8.99, 9.48	-0.74098	2	$C_7H_{11}O_8S^-$
209.04892	12.21	0.01047	1	$C_7H_{13}O_5S^-$
225.04337	14.52	-2.07343	1	$C_7H_{13}O_6S^-$
241.03879	9.03	0.17073	1	$C_7H_{13}O_7S^-$

Table S2. Continued.

[M-H]$^-$	Retention time	Error	DBE	Suggested formula
m / z	**min**	**ppm**		
227.05946	10.25, 13.54	-0.08213	0	$C_7H_{15}O_6S^-$
235.02808	8.75	-0.45041	3	$C_8H_{11}O_6S^-$
267.01797	7.61, 9.35, 9.63, 9.80	-0.13623	3	$C_8H_{11}O_8S^-$
283.01297	6.96	0.15597	3	$C_8H_{11}O_9S$
235.02808	8.75	-0.45041	2	$C_8H_{13}O_5S^-$
237.04382	19.55, 21.84, 28.47	-0.03733	2	$C_8H_{13}O_6S^-$
253.03857	12.78, 17.06, 28.46	-0.68160	2	$C_8H_{13}O_7S^-$
269.03357	12.64	-0.34179	2	$C_8H_{13}O_8S^-$
285.02872	5.64, 6.00, 7.39	0.49522	2	$C_8H_{13}O_9S^-$
223.06441	20.45	-0.71818	1	$C_8H_{15}O_5S^-$
239.05946	16.11, 20.07	-0.07801	1	$C_8H_{15}O_6S^-$
283.04944	19.56	0.44913	2	$C_9H_{15}O_8S^-$
299.08057	19.40	-0.15067	1	$C_{10}H_{19}O_8S^-$
287.02316	8.76	0.23068	6	$C_{11}H_{11}O_7S^-$
285.04376	17.36	-0.24517	6	$C_{12}H_{13}O_6S^-$
303.05435	16.52	-0.14830	5	$C_{12}H_{15}O_7S^-$
301.03891	17.43	0.54220	6	$C_{12}H_{13}O_7S^-$
299.05923	20.29	-0.82770	6	$C_{13}H_{15}O_6S^-$
315.05447	20.60	0.24481	6	$C_{13}H_{15}O_7S^-$

Table S3. Chemical formulae of organosulfates identified in previous studies.

[M-H]$^-$ *m / z*	DBE	Suggested formula	Possible precursor	Structure	Reference
209.0120	2	$C_6H_9O_6S^-$	diesel vapor	unknown	(Y.Wang et al., 2021)
182.999	1	$C_4H_7O_6S^-$	unknown	unknown	(Boris et al., 2016)
195.035	1	$C_6H_{11}O_5S^-$	unknown	unknown	
211.031	1	$C_6H_{11}O_6S^-$	unknown	unknown	
241.005	2	$C_6H_9O_8S^-$	unknown	unknown	
253.042	2	$C_8H_{13}O_7S^-$	limonene	unknown	
269.036	2	$C_8H_{13}O_8S^-$	unknown	unknown	
170.9969	0	$C_3H_7O_6S^-$	unknown	unknown	(Cai et al., 2020)
167.0384	0	$C_5H_{11}O_4S^-$	unknown	unknown	
176.9863	3	$C_5H_5O_5S^-$	unknown	unknown	
183.0333	0	$C_5H_{11}O_5S^-$	unknown	unknown	
231.018	0	$C_5H_{11}O_8S^-$	unknown	unknown	
181.054	0	$C_6H_{13}O_4S^-$	unknown	unknown	
188.9863	4	$C_6H_5O_5S^-$	unknown	unknown	
197.0489	0	$C_6H_{13}O_5S^-$	unknown	unknown	
209.0125	2	$C_6H_9O_6S^-$	unknown	unknown	
211.0282	1	$C_6H_{11}O_6S^-$	unknown	unknown	
211.0646	0	$C_7H_{15}O_5S^-$	unknown	unknown	
225.0438	1	$C_7H_{13}O_6S^-$	unknown	unknown	
207.0697	1	$C_8H_{15}O_4S^-$	unknown	unknown	
212.9863	6	$C_8H_5O_5S^-$	unknown	unknown	

Table S3. Continued.

[M-H]$^-$ *m / z*	DBE	Suggested formula	Possible precursor	Structure	Reference
221.0489	2	$C_8H_{13}O_5S^-$	unknown	unknown	(Cai et al., 2020)
223.0646	1	$C_8H_{15}O_5S^-$	unknown	unknown	
239.0595	1	$C_8H_{15}O_6S^-$	unknown	unknown	
239.0959	0	$C_9H_{19}O_5S^-$	unknown	unknown	
253.0751	1	$C_9H_{17}O_6S^-$	unknown	unknown	
297.0286	3	$C_9H_{13}O_9S^-$	unknown	unknown	
231.0697	3	$C_{10}H_{15}O_4S^-$	unknown	unknown	
237.1166	0	$C_{10}H_{21}O_4S^-$	unknown	unknown	
253.1115	0	$C_{10}H_{21}O_5S^-$	unknown	unknown	
251.1323	0	$C_{11}H_{23}O_4S^-$	unknown	unknown	
263.0959	2	$C_{11}H_{19}O_5S^-$	unknown	unknown	
265.1115	1	$C_{11}H_{21}O_5S^-$	unknown	unknown	
279.0908	2	$C_{11}H_{19}O_6S^-$	unknown	unknown	
281.1064	1	$C_{11}H_{21}O_6S^-$	unknown	unknown	
295.0857	2	$C_{11}H_{19}O_7S^-$	unknown	unknown	
265.1479	0	$C_{12}H_{25}O_4S^-$	unknown	unknown	
291.0908	3	$C_{12}H_{19}O_6S^-$	unknown	unknown	
293.1064	2	$C_{12}H_{21}O_6S^-$	unknown	unknown	
295.1221	1	$C_{12}H_{23}O_6S^-$	unknown	unknown	
309.1014	2	$C_{12}H_{21}O_7S^-$	unknown	unknown	
339.0755	3	$C_{12}H_{19}O_9S^-$	unknown	unknown	

Table S3. Continued.

[M-H]$^-$ *m / z*	DBE	Suggested formula	Possible precursor	Structure	Reference
293.1428	1	$C_{13}H_{25}O_5S^-$	unknown	unknown	(Cai et al., 2020)
307.1221	2	$C_{13}H_{23}O_6S^-$	unknown	unknown	
309.1377	1	$C_{13}H_{25}O_6S^-$	unknown	unknown	
323.117	2	$C_{13}H_{23}O_7S^-$	unknown	unknown	
323.1534	1	$C_{14}H_{27}O_6S^-$	unknown	unknown	
337.1327	2	$C_{14}H_{25}O_7S^-$	unknown	unknown	
321.1741	1	$C_{15}H_{29}O_5S^-$	unknown	unknown	
351.1483	2	$C_{15}H_{27}O_7S^-$	unknown	unknown	
335.1898	1	$C_{16}H_{31}O_5S^-$	unknown	unknown	
351.1847	1	$C_{16}H_{31}O_6S^-$	unknown	unknown	
373.0963	6	$C_{16}H_{21}O_8S^-$	unknown	unknown	

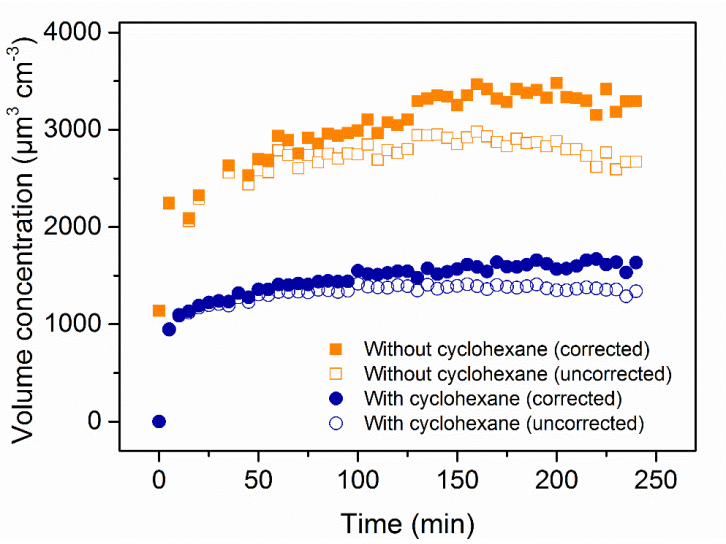

Figure S1. Particle volume concentration as a function of time during ozonolysis of cyclooctene with and without cyclohexane addition.

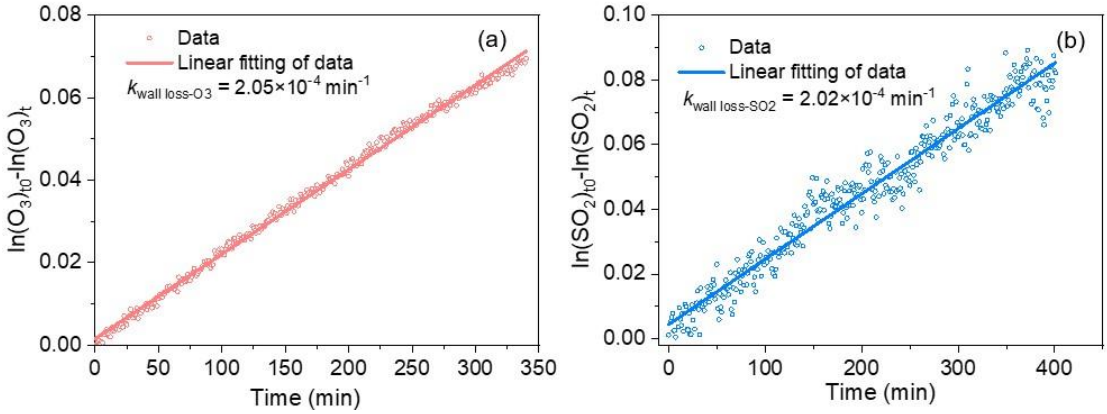

Figure S2. First-order wall losses of (a) O_3 and (b) SO_2 inside the chamber.

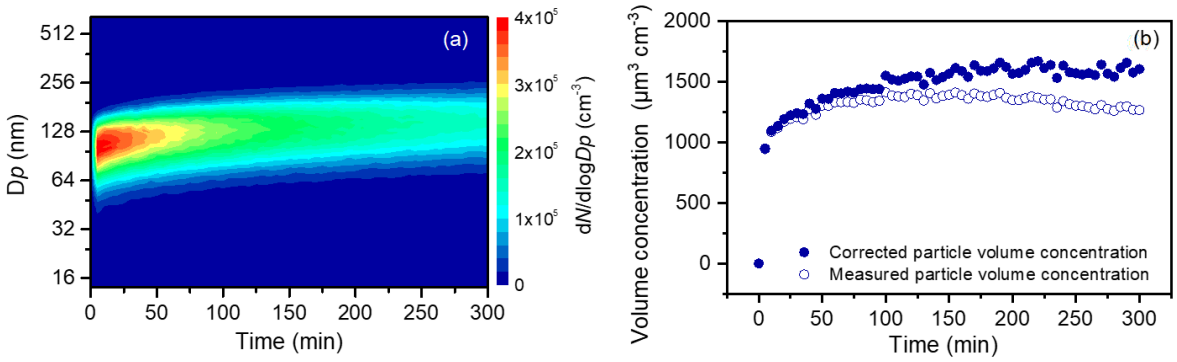

Figure S3. Particle formation from the ozonolysis of cyclooctene in the absence of SO_2. (a) Evolution of the particle number-diameter distribution. (b) Time series of particle volume concentration.

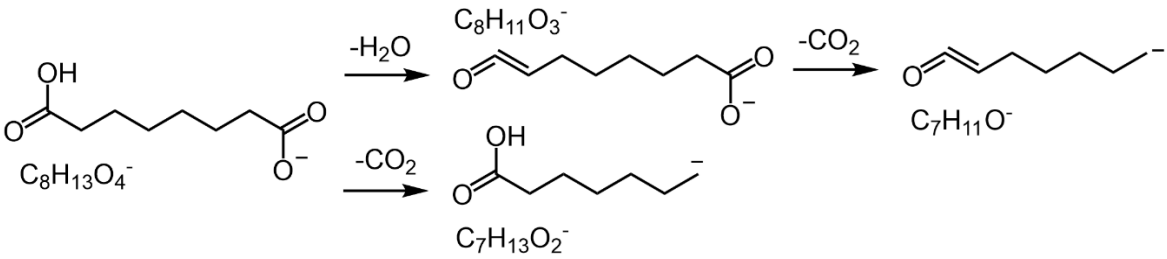

Figure S4. Proposed fragmentation routes of monomer $C_8H_{14}O_4$, largely based on schemes in Yasmeen et al. (2011).

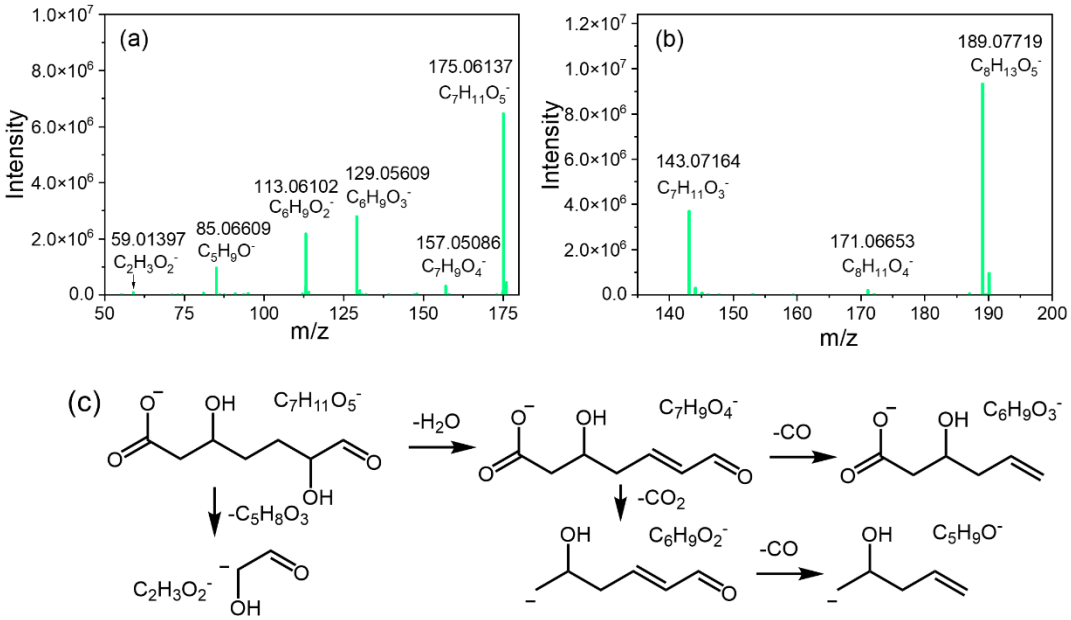

Figure S5. MS/MS spectra of monomers (a) $C_7H_{12}O_5$ and (b) $C_8H_{14}O_5$. Proposed fragmentation pathways of (c) $C_7H_{12}O_5$.

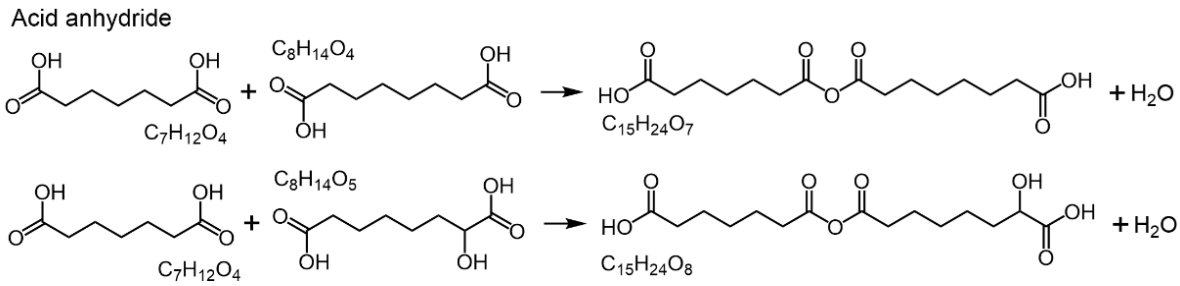

Figure S6. Formation mechanism of dimers $C_{15}H_{24}O_7$ and $C_{15}H_{24}O_8$.

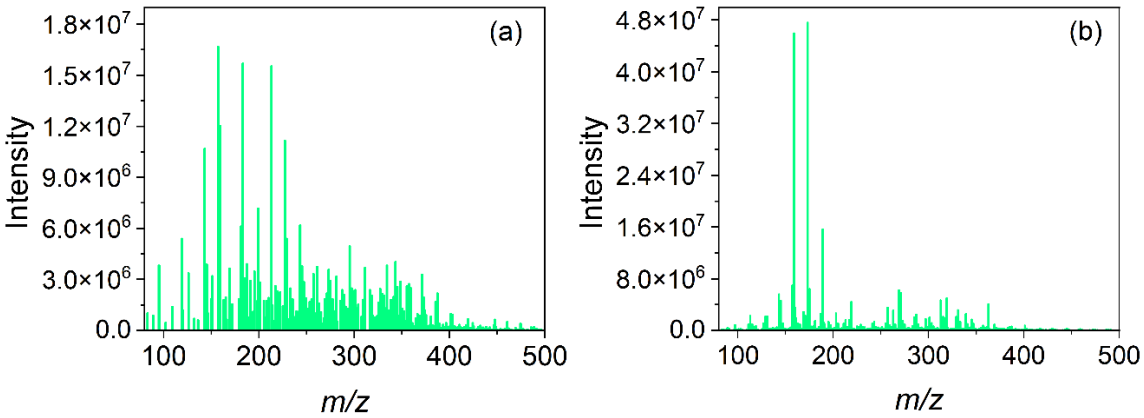

Figure S7. Mass spectra of methanol-extractable particles formed in the absence of SO_2. (a) Positive ion mode. (b) Negative ion mode.

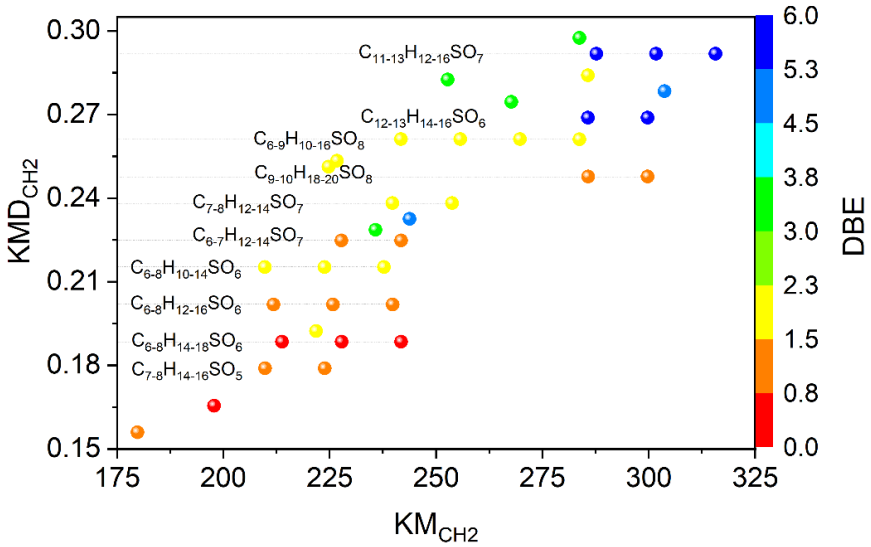

Figure S8. CH_2-Kendrick mass defect diagram of organosulfur compounds observed in particles formed in the presence of SO_2.

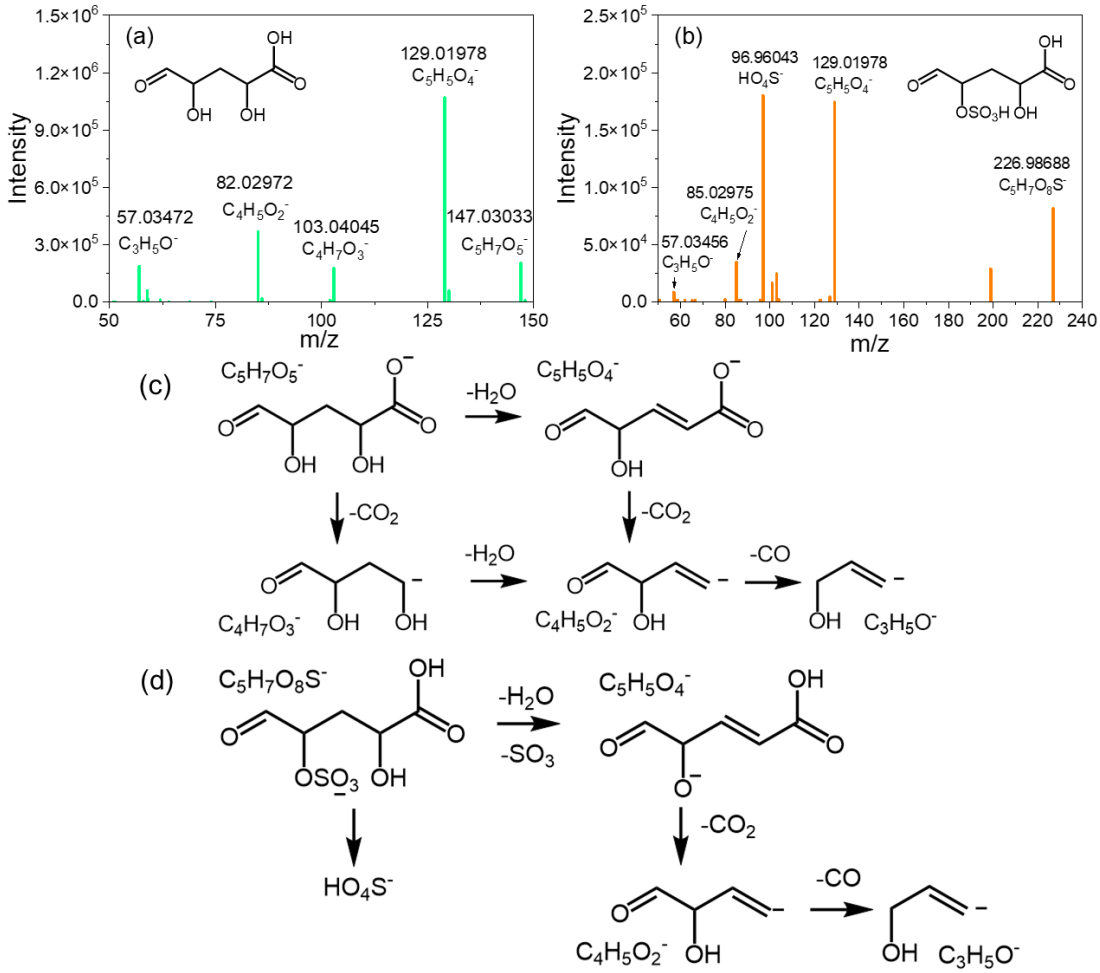

Figure S9. MS/MS spectra of (a) precursor $C_5H_8O_5$ and (b) organosulfate $C_5H_8O_8S$ from the ozonolysis of cyclooctene in the presence of SO_2. Corresponding fragmentation schemes of (c) $C_5H_8O_5$ and (d) $C_5H_8O_8S$.

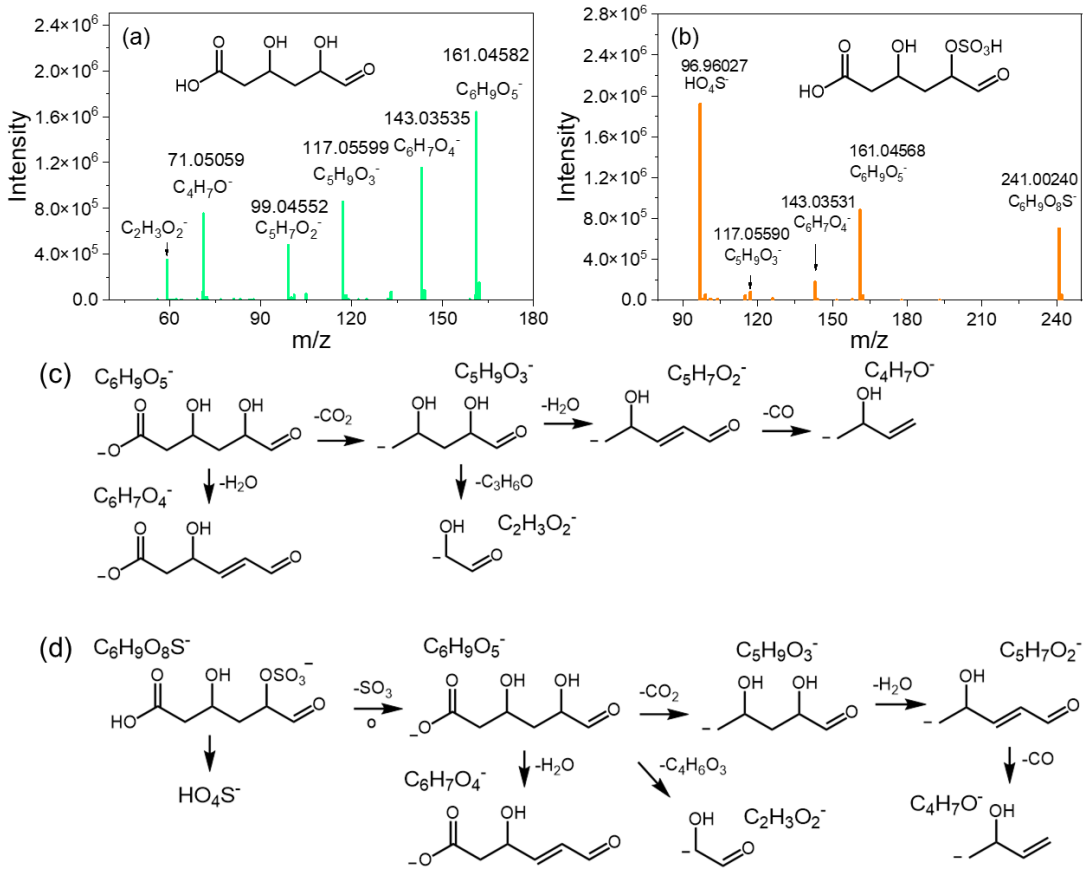

Figure S10. MS/MS spectra of (a) precursor $C_6H_{10}O_5$ and (b) organosulfate $C_6H_{10}O_8S$ from the ozonolysis of cyclooctene in the presence of SO_2. Corresponding fragmentation schemes of (c) $C_6H_{10}O_5$ and (d) $C_6H_{10}O_8S$.

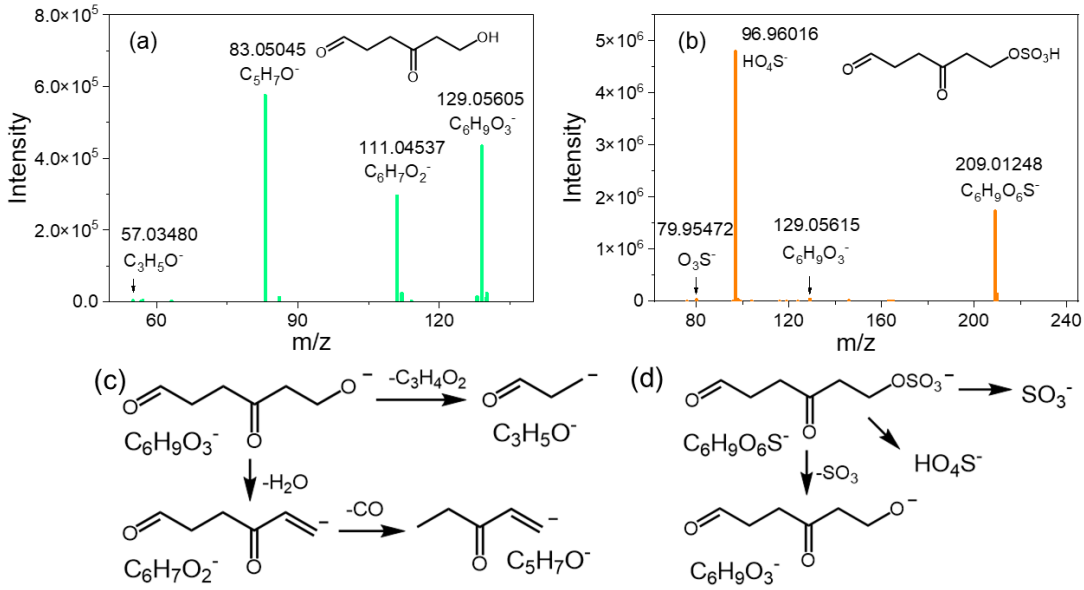

Figure S11. MS/MS spectra of (a) precursor $C_6H_{10}O_3$ and (b) organosulfate $C_6H_{10}O_6S$ from the ozonolysis of cyclooctene in the presence of SO_2. Corresponding fragmentation schemes of (c) $C_6H_{10}O_3$ and (d) $C_6H_{10}O_6S$.

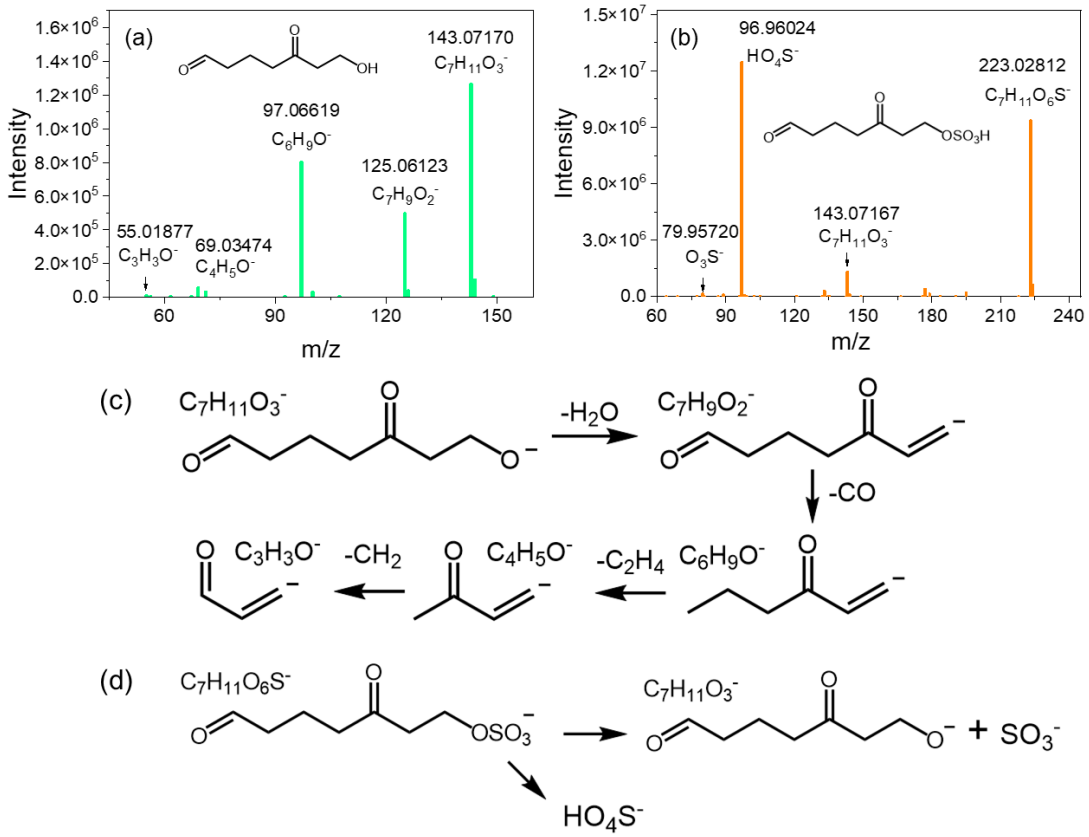

Figure S12. MS/MS spectra of (a) precursor $C_7H_{12}O_3$ and (b) organosulfate $C_7H_{12}O_6S$ from the ozonolysis of cyclooctene in the presence of SO_2. Corresponding fragmentation schemes of (c) $C_7H_{12}O_3$ and (d) $C_7H_{12}O_6S$.

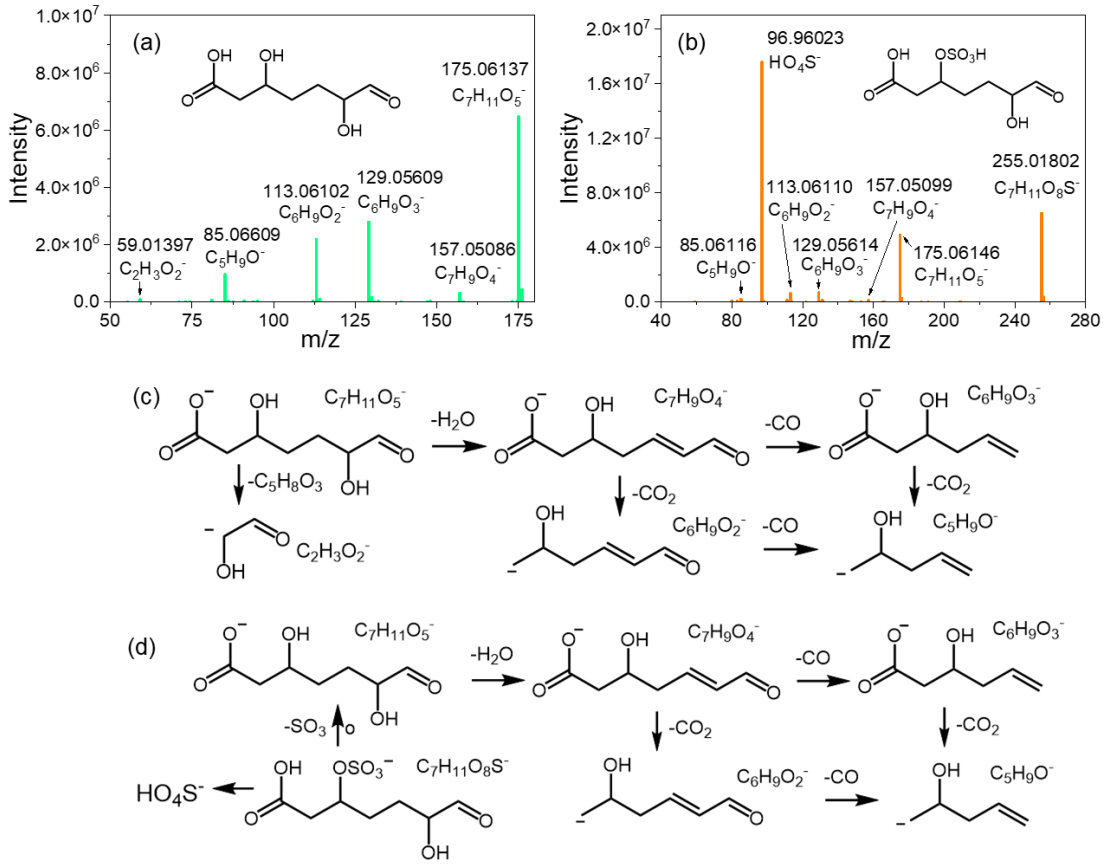

Figure S13. MS/MS spectra of (a) precursor $C_7H_{12}O_5$ and (b) organosulfate $C_7H_{12}O_8S$ from the ozonolysis of cyclooctene in the presence of SO_2. Corresponding fragmentation schemes of (c) $C_7H_{12}O_5$ and (d) $C_7H_{12}O_8S$.

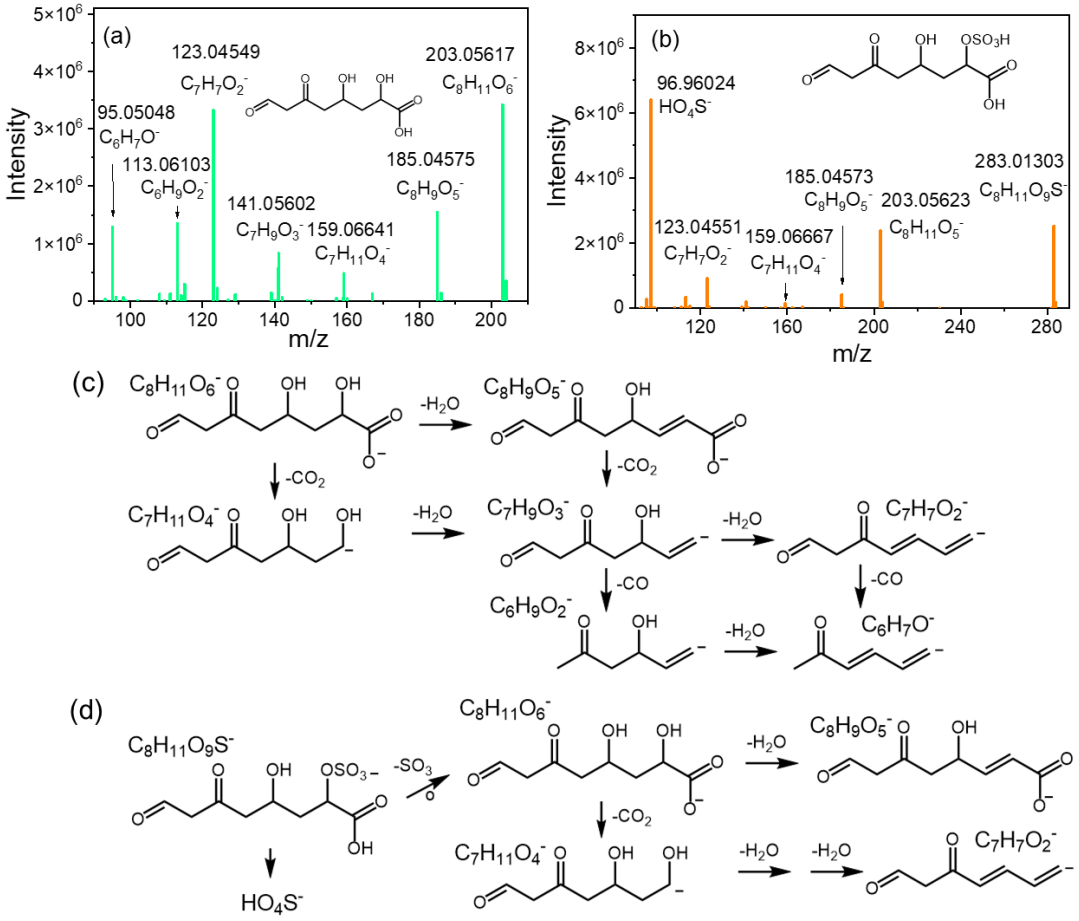

Figure S14. MS/MS spectra of (a) precursor $C_8H_{12}O_6$ and (b) organosulfate $C_8H_{12}O_9S$ from the ozonolysis of cyclooctene in the presence of SO_2. Corresponding fragmentation schemes of (c) $C_8H_{12}O_6$ and (d) $C_8H_{12}O_9S$.

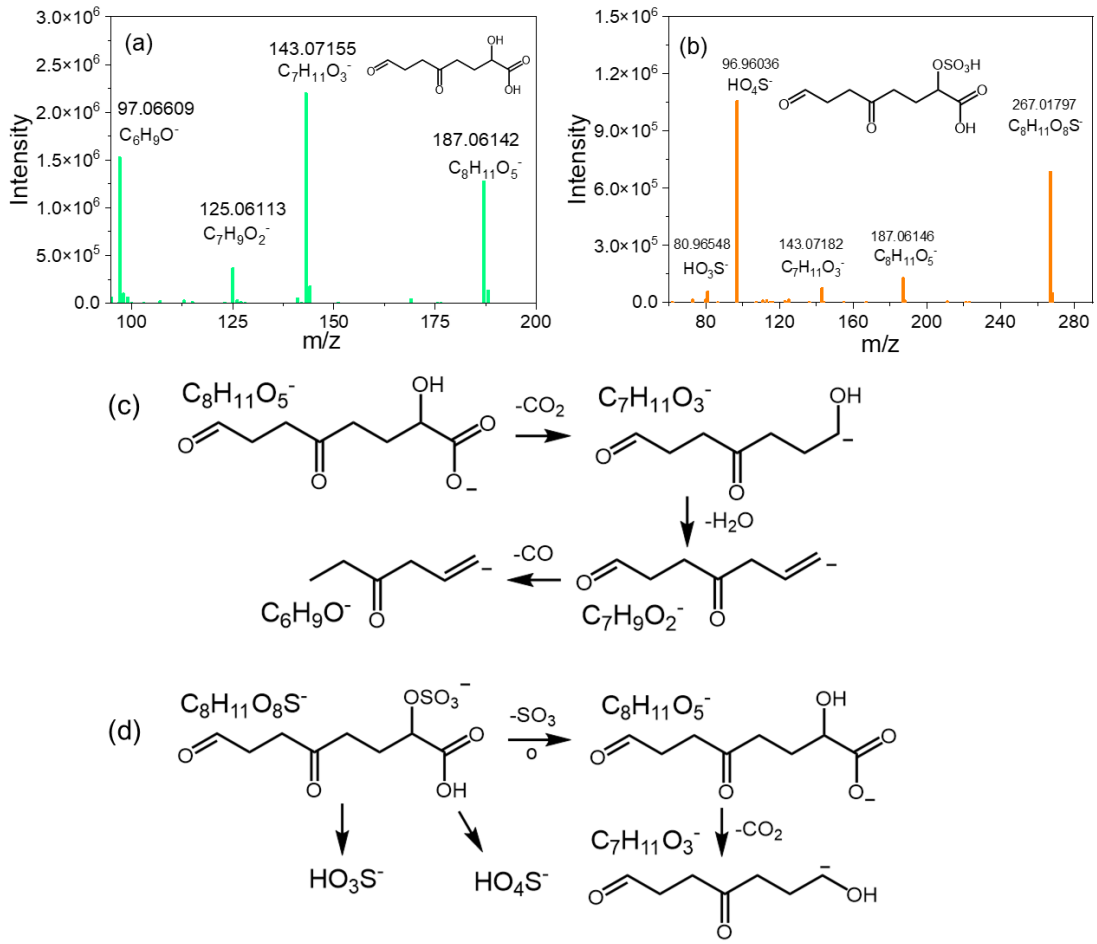

Figure S15. MS/MS spectra of (a) precursor $C_8H_{12}O_5$ and (b) organosulfate $C_8H_{12}O_8S$ from the ozonolysis of cyclooctene in the presence of SO_2. Corresponding fragmentation schemes of (c) $C_8H_{12}O_5$ and (d) $C_8H_{12}O_8S$.

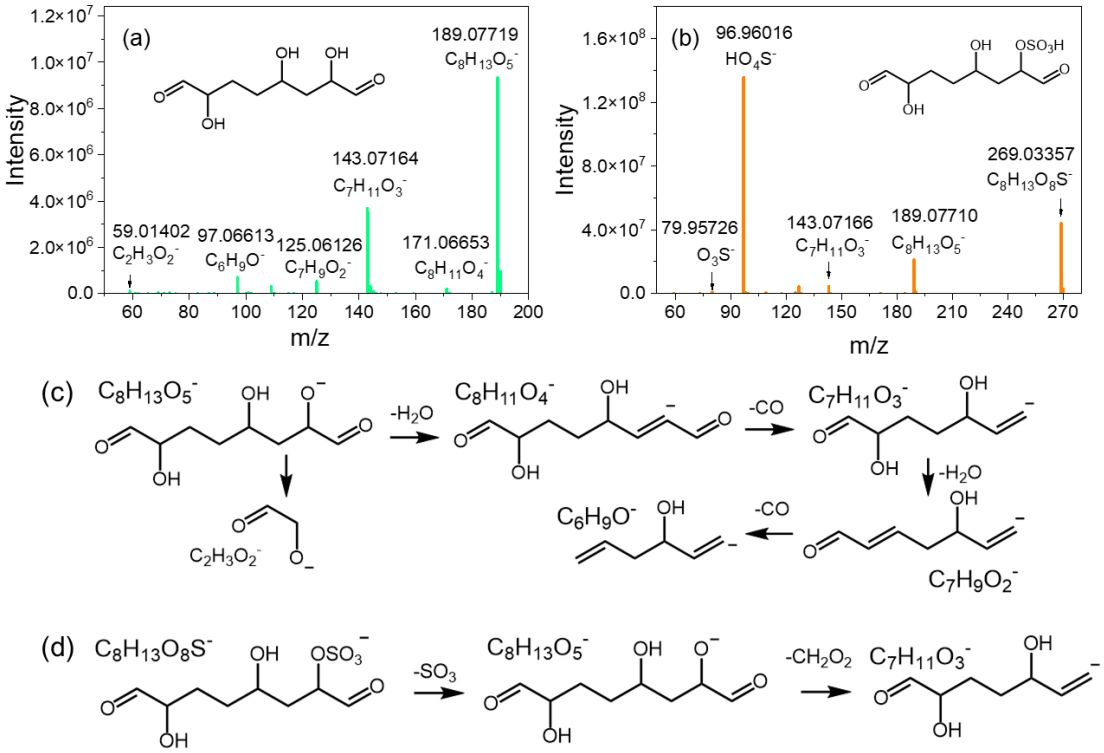

Figure S16. MS/MS spectra of (a) precursor $C_8H_{14}O_5$ and (b) organosulfate $C_8H_{14}O_8S$ from the ozonolysis of cyclooctene in the presence of SO_2. Corresponding fragmentation schemes of (c) $C_8H_{14}O_5$ and (d) $C_8H_{14}O_8S$.

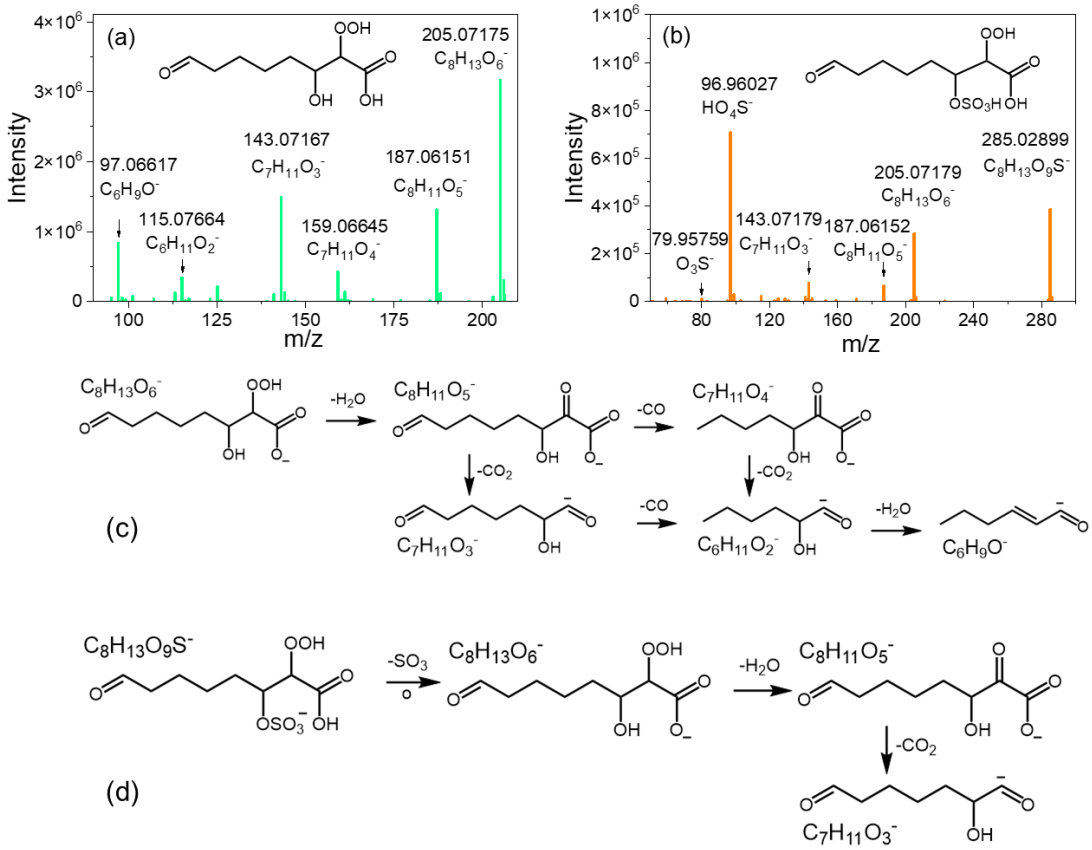

Figure S17. MS/MS spectra of (a) precursor $C_8H_{14}O_6$ and (b) organosulfate $C_8H_{14}O_9S$ from the ozonolysis of cyclooctene in the presence of SO_2. Corresponding fragmentation schemes of (c) $C_8H_{14}O_6$ and (d) $C_8H_{14}O_9S$.

Reference

Boris, A. J., Lee, T., Park, T., Choi, J., Seo, S. J., and Collett Jr, J. L.: Fog composition at Baengnyeong Island in the eastern Yellow Sea: detecting markers of aqueous atmospheric oxidations, Atmos. Chem. Phys., 16, 437-453, 10.5194/acp-16-437-2016, 2016.

Cai, D., Wang, X., Chen, J., and Li, X.: Molecular characterization of organosulfates in highly polluted atmosphere using ultra-high-resolution mass spectrometry, J. Geophys. Res.-Atmos., 125, e2019JD032253, 10.1029/2019jd032253, 2020.

Hung, H. M., Chen, Y. Q., and Martin, S. T.: Reactive aging of films of secondary organic material studied by infrared spectroscopy, J. Phys. Chem. A, 117, 108-116, 10.1021/jp309470z, 2013.

Krechmer, J. E., Day, D. A., Ziemann, P. J., and Jimenez, J. L.: Direct Measurements of Gas/Particle Partitioning and Mass Accommodation Coefficients in Environmental Chambers, Environ. Sci. Technol., 51, 11867-11875, 10.1021/acs.est.7b02144, 2017.

Lal, V., Khalizov, A. F., Lin, Y., Galvan, M. D., Connell, B. T., and Zhang, R.: Heterogeneous reactions of epoxides in acidic media, J. Phys. Chem. A, 116, 6078-6090, 10.1021/jp2112704, 2012.

Lin, Y. H., Budisulistiorini, H., Chu, K., Siejack, R. A., Zhang, H. F., Riva, M., Zhang, Z. F., Gold, A., Kautzman, K. E., and Surratt, J. D.: Light-Absorbing Oligomer Formation in Secondary Organic Aerosol from Reactive Uptake of Isoprene Epoxydiols, Environ. Sci. Technol., 48, 12012-12021, 10.1021/es503142b, 2014.

Liu, Y., Liggio, J., Staebler, R., and Li, S. M.: Reactive uptake of ammonia to secondary organic aerosols: kinetics of organonitrogen formation, Atmos. Chem. Phys., 15, 13569-13584, 10.5194/acp-15-13569-2015, 2015.

Matsunaga, A. and Ziemann, P. J.: Gas-Wall Partitioning of Organic Compounds in a Teflon Film Chamber and Potential Effects on Reaction Product and Aerosol Yield Measurements, Aerosol Sci. Technol., 44, 881-892, 10.1080/02786826.2010.501044, 2010.

McMurry, P. H. and Grosjean, D.: Gas and aerosol wall losses in Teflon film smog chambers, Environ. Sci. Technol., 19, 1176-1182, 10.1021/es00142a006, 1985.

Sarrafzadeh, M., Wildt, J., Pullinen, I., Springer, M., Kleist, E., Tillmann, R., Schmitt, S. H., Wu, C., Mentel, T. F., Zhao, D., Hastie, D. R., and Kiendler-Scharr, A.: Impact of NO_x and OH on secondary organic aerosol formation from β-pinene photooxidation, Atmos. Chem. Phys., 16, 11237-11248,

10.5194/acp-16-11237-2016, 2016.

Sax, M., Zenobi, R., Baltensperger, U., and Kalberer, M.: Time resolved infrared spectroscopic analysis of aerosol formed by photo-oxidation of 1,3,5-trimethylbenzene and alpha-pinene, Aerosol Sci. Technol., 39, 822-830, 10.1080/02786820500257859, 2005.

Tammer, M.: G. Sokrates: Infrared and Raman characteristic group frequencies: tables and charts, Colloid and Polymer Science, 283, 235-235, 10.1007/s00396-004-1164-6, 2004.

Tang, M. J., Shiraiwa, M., Pöschl, U., Cox, R. A., and Kalberer, M.: Compilation and evaluation of gas phase diffusion coefficients of reactive trace gases in the atmosphere: Volume 2. Diffusivities of organic compounds, pressure-normalised mean free paths, and average Knudsen numbers for gas uptake calculations, Atmos. Chem. Phys., 15, 5585-5598, 10.5194/acp-15-5585-2015, 2015.

Wang, Y., Zhao, Y., Wang, Y., Yu, J.-Z., Shao, J., Liu, P., Zhu, W., Cheng, Z., Li, Z., Yan, N., and Xiao, H.: Organosulfates in atmospheric aerosols in Shanghai, China: seasonal and interannual variability, origin, and formation mechanisms, Atmos. Chem. Phys., 21, 2959-2980, 10.5194/acp-21-2959-2021, 2021.

Yasmeen, F., Szmigielski, R., Vermeylen, R., Gomez-Gonzalez, Y., Surratt, J. D., Chan, A. W., Seinfeld, J. H., Maenhaut, W., and Claeys, M.: Mass spectrometric characterization of isomeric terpenoic acids from the oxidation of alpha-pinene, beta-pinene, d-limonene, and Delta3-carene in fine forest aerosol, J Mass Spectrom, 46, 425-442, 10.1002/jms.1911, 2011.

Zhang, X., Cappa, C. D., Jathar, S. H., McVay, R. C., Ensber, J. J., Kleeman, M. J., and Seinfeld, J. H.: Influence of vapor wall loss in laboratory chambers on yields of secondary organic aerosol, P. Natl. Acad. Sci. USA, 111, 5802-5807, 2014.